

# Multifunctional Hybrid Nanocarrier: Magnetic CNTs Ensheathed with Mesoporous Silica for Drug Delivery and Imaging System

Rajendra K. Singh,<sup>†,‡</sup> Kapil D. Patel,<sup>†,‡</sup> Jung-Ju Kim,<sup>†,‡</sup> Tae-Hyun Kim,<sup>†,‡</sup> Joong-Hyun Kim,<sup>†,‡</sup> Ueon Sang Shin,<sup>†,‡</sup> Eun-Jung Lee,<sup>†,‡</sup> Jonathan C. Knowles,<sup>‡,§</sup> and Hae-Won Kim<sup>†,‡,⊥,\*</sup>

<sup>†</sup>Institute of Tissue Regeneration Engineering (ITREN) and <sup>⊥</sup>Department of Biomaterials Science, School of Dentistry, Dankook University, Cheonan 330-714, South Korea

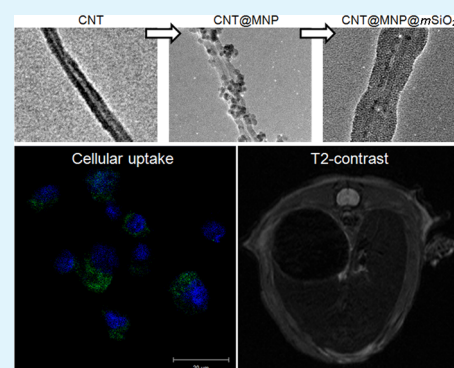
<sup>‡</sup>Department of Nanobiomedical Science & BK21 PLUS NBM Global Research Center for Regenerative Medicine, Dankook University, Cheonan 330-714, South Korea

<sup>§</sup>Division of Biomaterials and Tissue Engineering, Eastman Dental Institute, University College London, 256 Gray's Inn Road, London WC1X 8LD, United Kingdom

## S Supporting Information

**ABSTRACT:** Here we communicate the development of a novel multifunctional hybrid nanomaterial, magnetic carbon nanotubes (CNTs) ensheathed with mesoporous silica, for the simultaneous applications of drug delivery and imaging. Magnetic nanoparticles (MNPs) were first decorated onto the multiwalled CNTs, which was then layered with mesoporous silica (*mSiO*<sub>2</sub>) to facilitate the loading of bioactive molecules to a large quantity while exerting magnetic properties. The hybrid nanomaterial showed a high mesoporosity due to the surface-layered *mSiO*<sub>2</sub>, and excellent magnetic properties, including magnetic resonance imaging in vitro and in vivo. The mesoporous and magnetic hybrid nanocarriers showed high loading capacity for therapeutic molecules including drug gentamicin and protein cytochrome C. In particular, genetic molecule siRNA was effectively loaded and then released over a period of days to a week. Furthermore, the hybrid nanocarriers exhibited a high cell uptake rate through magnetism, while eliciting favorable biological efficacy within the cells. This novel hybrid multifunctional nanocarrier may be potentially applicable as drug delivery and imaging systems.

**KEYWORDS:** multifunctional nanocarrier, CNTs, magnetic property, cell uptake, drug delivery, mesoporosity



## INTRODUCTION

Carbon nanotubes (CNTs), first discovered in 1991,<sup>1</sup> have found potential applications in a variety of fields because of their unique optical, electronic, and mechanical properties.<sup>2</sup> Great interests have recently arisen in their biomedical utility, mainly as a carrier of therapeutic molecules.<sup>3–5</sup> Because of their size in the nanoscale regime, the consequent ultrahigh surface area, and the possible surface functional group modification, CNTs are an attractive platform for the delivery of drugs and genes into the target cells. Although concerns of biocompatibility (cell and tissue toxicity) of CNTs have been raised as a practical issue, and many in-depth studies of this are still ongoing, it is generally accepted that when the surface of CNTs is properly functionalized (modified), a significant improvement in the cell and tissue compatibility can be achieved.

Another emerging issue of CNTs for use in biomedical areas is to provide multifunctionality. One example of this is to endow magnetic properties, which has been implemented through the combination of magnetic nanoparticles (MNPs) with CNTs.<sup>6–9</sup> The MNP-decorated CNT (CNT@MNP) has shown excellent magnetic properties, while preserving the merits of CNTs, potentially extending the possible uses in cell

imaging and diagnostics associated with MNPs.<sup>10–12</sup> Although the specific performance of the CNT@MNP in medical fields has not been elucidated, potential applications in therapeutics–diagnostics (“theranostics”) are expected.

Therefore, here we first focus on utilizing this CNT@MNP more efficiently, through coating with silica. In particular, the silica coating layer was developed to have a mesoporous structure, aiming to improve drug loading and delivery capacity. In fact, the silica (mesoporous or nonmesoporous) has been a potent composition to cover relatively toxic nanomaterials, such as quantum dots, CNTs and MNPs,<sup>13–15</sup> creating a more biocompatible interface in the interaction with cells and tissues. One recent work has reported the decoration of CNTs with magnetic silica nanoparticles.<sup>16</sup>

To the best of our knowledge, the development of mesoporous silica-layered CNT@MNP (CNT@MNP@mSiO<sub>2</sub>) has yet to be implemented. Here, we assess the physicochemical and magnetic properties of CNT@MNP@

Received: July 14, 2013

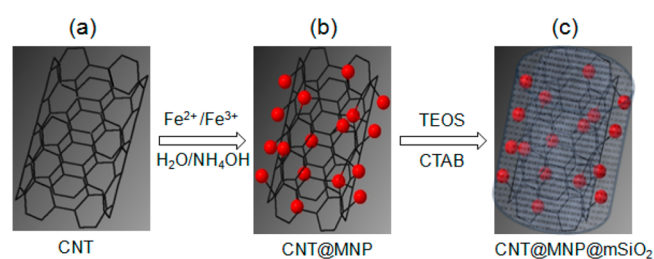
Accepted: January 29, 2014

Published: January 29, 2014

$m\text{SiO}_2$ , and examine the capacity to enable imaging contrast under a magnetic resonance in vitro and in vivo. Furthermore, the potential of the nanomaterials in loading therapeutic molecules is addressed using three model therapeutics, cytochrome *c*, gentamicin, and small interfering RNA (siRNA). Finally, the intracellular uptake of the siRNA-loaded nanocarrier through a magnetofection is also investigated.

Scheme 1 depicts the synthesis scheme of CNT@MNP@mSiO<sub>2</sub> hybrid nanocarrier. First, amine-functionalized CNTs

**Scheme 1. Schematic Illustration Showing the Synthesis of Nanocarrier Mesoporous Magnetic Carbon Nanotubes Ensheathed with Mesoporous Silica (CNT@MNP@mSiO<sub>2</sub>): (a) CNT Serving As a Template, (b) Magnetite Nanoparticles (MNP, red dots) Decorated on the CNT Surface, and (c) Mesoporous Silica (mSiO<sub>2</sub>) Covering the Surface of CNT@MNP**



were exposed to  $\text{Fe}^{2+}$  and  $\text{Fe}^{3+}$  solution which hydrolyzed into  $\beta\text{-FeOOH}$  in neutral water (pH 7.0) at room temperature. After this, uniform nanoparticles ( $\beta\text{-FeOOH}$ ) are present on the surfaces of CNTs templates, because  $\beta\text{-FeOOH}$  colloids with a surface full of hydroxyl anion groups have a strong propensity to electrostatically attract amino-modified CNT molecules. In basic conditions,  $\beta\text{-FeOOH}$  transforms to  $\text{Fe}_3\text{O}_4$  magnetite phase. Thereafter, a silica layer with a desired thickness is deposited on the surface of the magnetite core and CNTs by sol-gel polymerization of tetraethyl orthosilicate (TEOS).

## EXPERIMENTAL PROCEDURES

**CNTs and Amination.** CNTs (multiwalled, grade >95% pure, 15–20 nm outer diameter, 10–20  $\mu\text{m}$  length, EM-Power Co., LTD, Korea,) were first functionalized with carboxylic group. One gram of raw CNTs was added to a 1:1 mixture of concentrated nitric acid and/sulfuric acid and then refluxed at 80 °C for 2 days. The carboxylated CNTs were then diluted with distilled water and filtered through a filter-paper (Millipore, 0.2  $\mu\text{m}$  polycarbonate). After the acid treatment and filtration processes, the size of CNTs decreased substantially. The carboxylated CNTs were amine-functionalized with 3-aminopropyltriethoxysilane (APTES, Sigma-Aldrich) in the presence of 1-ethyl-3-(3-dimethylaminopropyl) carbodiimide (EDC, Sigma-Aldrich). The aminated CNTs were washed fully with distilled water and ethanol, and then dried under vacuum for further uses.

**Preparation of CNT@MNP and CNT@MNP@mSiO<sub>2</sub>.** Amine-functionalized CNTs (30 mg) were added either to ferrous chloride tetrahydrate ( $\text{FeCl}_2 \cdot 4\text{H}_2\text{O}$ , Sigma-Aldrich) in 1 M HCl or to ferric chloride hexahydrate ( $\text{FeCl}_3 \cdot 6\text{H}_2\text{O}$ , Sigma-Aldrich), which were then mixed ( $\text{Fe}^{2+}/\text{Fe}^{3+} = 1/2$ ) and sonicated for 1 h. After this, the mixture was added dropwise into 100 mL of 1.5 M NaOH solution with vigorous stirring. After 30 min, the resulting precipitate was isolated by magnetic

field and the solution was decanted after centrifugation at 8000 rpm and dried at 40 °C to prepare CNT decorated with MNPs (CNT@MNP). All steps were performed under nitrogen gas to avoid oxidation.

The CNT@MNP was covered with mesoporous silica via a facile sol-gel coating pathway. The CNT@MNP (15 mg) was added to the mixture solution of 200 mg of cetrimonium bromide (CTAB, Sigma-Aldrich), 200 mL of ethanol, 20 mL of distilled water, and 2.4 mL of ammonia (25%), and then sonicated for 3 h. Silanization of CNT@MNP was carried out by a dropwise addition of 200  $\mu\text{L}$  of tetraethyl orthosilicate (TEOS, Sigma-Aldrich) dissolved in 20 mL of ethanol while stirring for 24 h. The solution was decanted and the CNT@MNP ensheathed with silica were treated with 20 mg of ammonium nitrate solution in 40 mL of deionized water at 60 °C overnight. After centrifugation, the samples were washed with ethanol and distilled water, and then dried under vacuum to obtain CNT@MNP@mSiO<sub>2</sub>.

The surface of CNT@MNP@mSiO<sub>2</sub> was further amine-functionalized with APTES for selective use of drug loading. CNT@MNP@mSiO<sub>2</sub> nanoparticles of 0.1 g of were added to 50 mL of toluene and sonicated for 30 min to a homogeneous solution. One milliliter of APTES was added to this solution and then refluxed at 80 °C for 24 h, which was followed by a centrifugation at 8000 rpm for 5 min and stringent washing with toluene and ethanol. The product was dried in an oven at 80 °C for 24 h.

**Characterizations.** The crystal structure was determined by X-ray diffraction (XRD; Ragaku). The samples were scanned in the range of diffraction angle  $2\theta = 5\text{--}60^\circ$  at a rate of  $2^\circ \text{min}^{-1}$  with a step width of  $0.02^\circ 2\theta$  using Cu  $K\alpha 1$  radiation at 40 kV and 40 mA. Fourier transform infrared spectroscopy (FT-IR; Varian 640-IR) was used to determine chemical bond status of the samples. For each spectrum, 20 scans in the wavenumber of  $400\text{--}2000 \text{ cm}^{-1}$  were recorded in the transmission mode by potassium bromide (KBr) pellet method. The specific surface area was calculated by the Brunauer-Emmett-Teller (BET) method. Pore size distribution was measured from the Barret-Joner-Halenda (BJH) method. The surface electrostatic property ( $\zeta$ -potential) of the samples was studied using a Zetasizer Nano apparatus (Malvern Instruments) at pH 7.0 and 25 °C. The morphology of the samples was characterized by transmission electron microscope (TEM, JEOL-7100). The size of samples was analyzed by a particle size analyzer (Zetasizer Nano ZS, Malvern Instruments, UK) based on a dynamic light scattering (DLS) measurement.

**Magnetic Properties and MRI Contrast Imaging.** The magnetic properties of the samples in powder form were studied by superconducting quantum interference device (SQUID, Quantum Design MPMS-XL7) in an applied magnetic field of  $\pm 20 \text{ kOe}$  at room temperature. Magnetic properties of the particles were evaluated in terms of saturation magnetization and hysteresis loop area.

Magnetic resonance imaging (MRI) experiments of the samples were performed at 25 °C in a clinical MR scanner (BioSpec 47/40; Bruker; 4.7 T). CNT@MNP@mSiO<sub>2</sub> hybrids were suspended in tubes of water (1 mL) at iron concentration of 0.0156, 0.0328, 0.0770, 0.1012, 0.1526, 0.2068, 0.3011 mM. The tubes were placed into the MR scanner and a number of MR sequence was run.  $T_2$  relaxation time was determined from a spin-echo sequence (32 echoes, repetition time (TR) of 10000 ms, echo time (TE) of 7.5–256 ms, matrix size of  $128 \times 128$ , slice thickness of 2 mm, field of view of  $50 \times 60 \text{ mm}^2$ , and

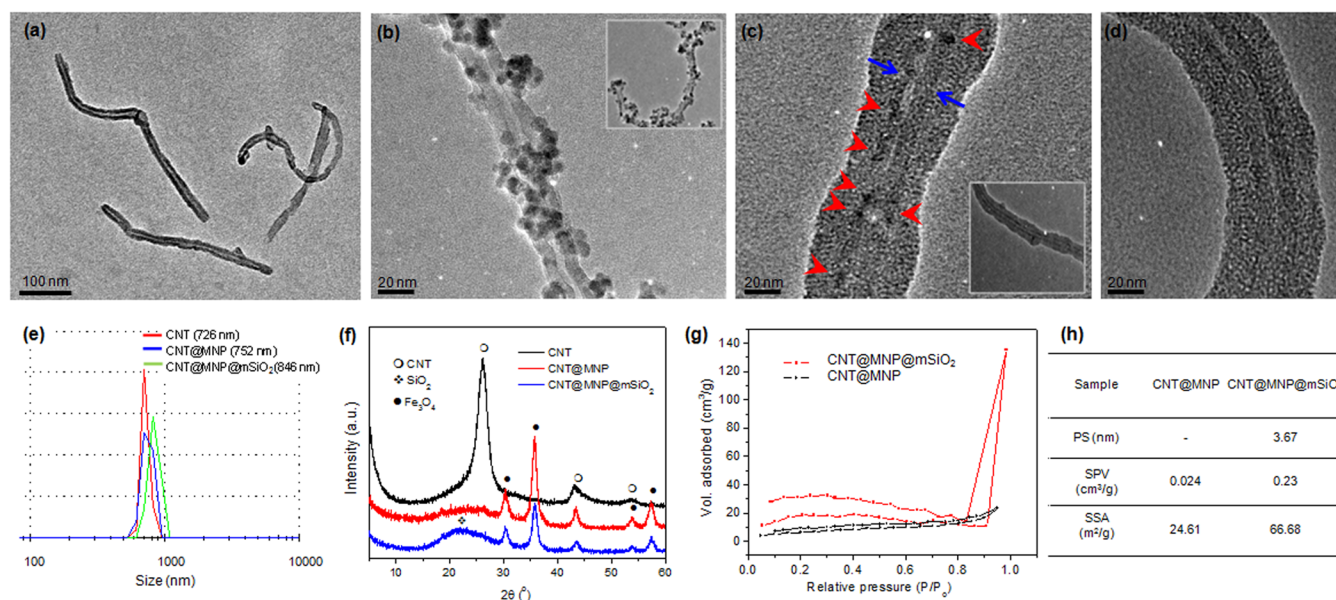


**Figure 1.** TEM images of the (a) CNTs used as a template, (b) CNT decorated with MNPs (CNT@MNP), and (c) further ensheathed with mesoporous silica (CNT@MNP@mSiO<sub>2</sub>). Inset images are low magnification. MNPs have sizes of  $\sim 12$  nm on average, and multiwalled CNTs have a wall thickness of  $\sim 14$  nm and a total width of 35 nm. The outer silica was highly mesoporous, covering the MNP-decorated CNT surface uniformly and completely. Average silica shell thickness was 18 nm. Arrows indicate silica shell and arrowheads point to embedded MNPs. (d) Image of mSiO<sub>2</sub>-ensheathed CNT without MNP decoration, for the purpose of comparison. (e) DLS measured hydrodynamic size of the samples. (f) XRD pattern of the mesoporous magnetic CNT, presenting peaks mainly of CNT ( $2\theta = 25.5^\circ$ ), MNPs ( $2\theta = 36, 38, 54,$  and  $57^\circ$ ), and a broadened silica peak at  $2\theta = 22.5^\circ$ , demonstrating the coverage of CNT@MNP by the silica layer. (g) N<sub>2</sub> adsorption/desorption isotherm curve of the mesoporous magnetic CNT, in comparison with that of CNT@MNP without silica layering. (h) Characteristics of the mesopore structure, including mesopore size, its volume and surface area, are also presented, comparing CNT@MNP and CNT@MNP@mSiO<sub>2</sub>.

number of acquisition of 1). Data were fitted by using a Levenberg–Marquardt method with Matlab (MathWorks Inc.) and Origin (OriginLab Corp.) program.

**Drug and Protein Loading.** The loading of a series of biomolecules onto the developed CNT@MNP@mSiO<sub>2</sub> was investigated. Two representative biomolecules, including protein (cytochrome c; cyt C) and drug (gentamicin sulfate; GS) were chosen. In each experiment, 1 mg of CNT@MNP@mSiO<sub>2</sub> was suspended in buffer solution (pH 7.4) with different concentration of the biomolecules, and ultrasonicated for 10 s and left for 2 h at 37 °C. The equilibrated samples were centrifuged for 4 min at 8000 rpm at each time point. The amount of biomolecules adsorbed was calculated by subtracting the amount remained in the supernatant liquid from the amount initially added. For cyt C, ultraviolet–visible spectrophotometer (Biochrom) was used to measure the absorbance at 408 nm. In case of GS, *o*-phthalaldehyde was used as a derivatizing agent to react with the amino groups of gentamicin and yield chromophoric products. The reaction was carried out by making 1 mL of GS sample in solution react with 1 mL of isopropanol and 1 mL of *o*-phthalaldehyde reagent. After mixing, the concentration of GS was determined by the UV absorbance at 332 nm.

**siRNA Loading and Cell Uptake Study.** For the loading study of genetic molecules, small interfering RNA (siRNA) was used. Different concentration of CNT@MNP@mSiO<sub>2</sub> (10, 20, and 40  $\mu$ g) were reacted with 1  $\mu$ g of fluorescein isothiocyanate (FITC)-conjugated negative control siRNA (Bioneer, Korea) within 1 mL of release medium (RNase-free distilled water) for 60 min at room temperature. After the complexation reaction, the release medium was centrifuged at 14 000 rpm and 4 °C for 30 min, and the amount of FITC-conjugated siRNA in the supernatant was determined using a SpectraMax M2e multi-

detection microplate reader (Molecular Device). Samples were tested in triplicate at each condition.

For the delivery of the siRNA-complexed CNT@MNP@mSiO<sub>2</sub> into cells, 2  $\mu$ g of FITC-conjugated siRNA and 20  $\mu$ g of CNT@MNP@mSiO<sub>2</sub> were mixed for 60 min, which was used as a siRNA mixture. MC3T3-E1 (ATCC) cells were seeded at  $1 \times 10^5$  cells in each well of six-well plates and the Opti-MEM mixture (Invitrogen) was added to each well at a concentration of 2  $\mu$ g/mL and left for different time points (from 10 to 120 min). In particular, magnetism-induced uptake test was also carried out using a magnetofection kit as another experimental group. After the cell uptake, the cells were harvested and assessed. As a control group, siRNA (FITC-conjugated form) only was also used, where the concentration was 2  $\mu$ g, the same as that used for the loading onto nanocarriers.

To quantify the population of siRNA-delivered cells, cells were fixed with 4% paraformaldehyde solution for 30 min on the coating slide glass. The fixed cells were washed with cold PBS (4 °C) and mounted on a cover glass. Fluorescent images were observed and analyzed using a LSM 510 laser-scanning confocal microscope (Carl Zeiss). Cells were counterstained with DAPI (Invitrogen) to observe the nuclei. Quantification of cell-uptake efficiency was also analyzed using a FACSCalibur flow cytometer (BD Biosciences). Data acquired for 10 000 cells in each sample were analyzed using the CellQuest Pro software (BD Biosciences).

**In Vivo Imaging Study.** After confirming the in vitro images of samples, the in vivo study in mice was conducted. T2-weighted MRI images were obtained using 4.7 T MRI system (Bruker, Germany) under operating conditions (sequence value TE/TR = 36/3500 ms, matrix size = 256  $\times$  256, and field of view = 35  $\times$  35 mm<sup>2</sup>), before and after the injection of CNT@MNP@mSiO<sub>2</sub> nanocarriers. ICR mice (male, weight 25 g) were

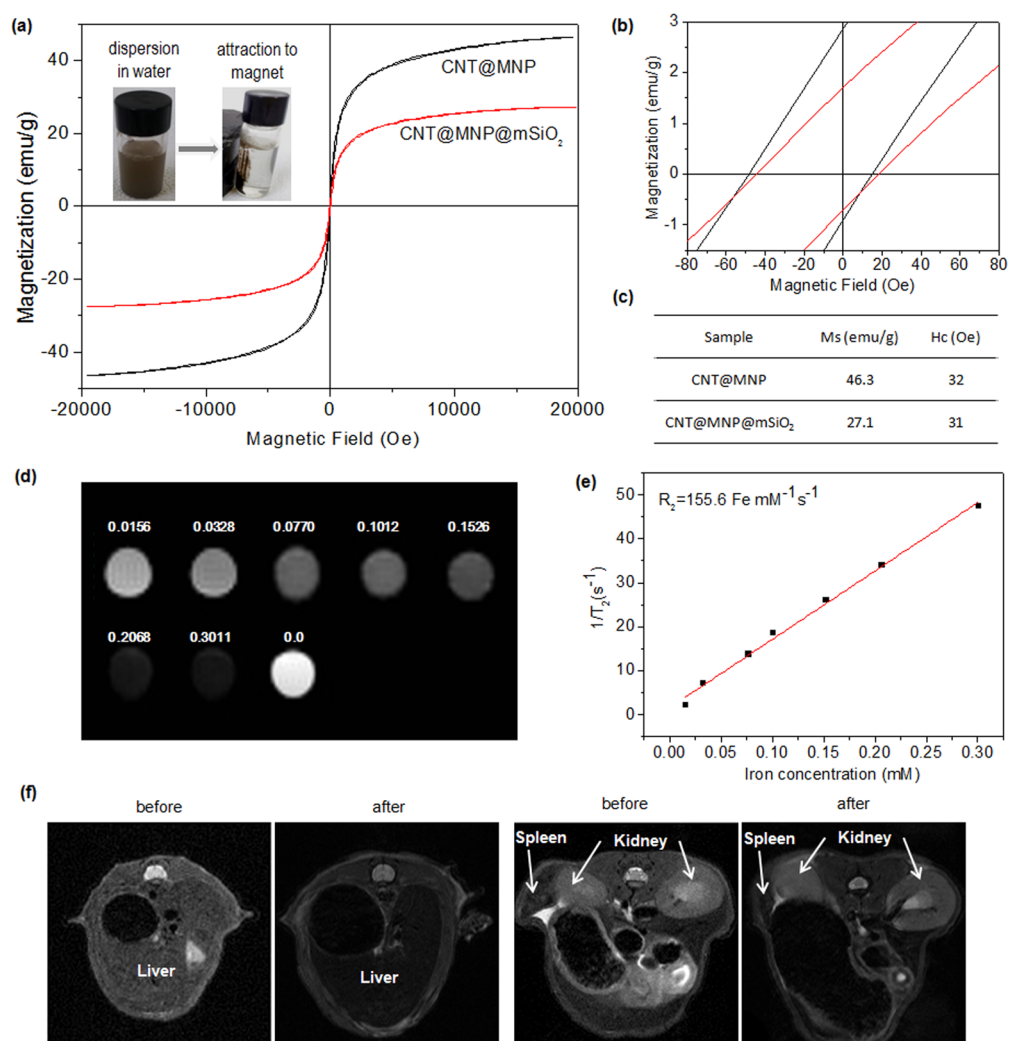


**Figure 2.** Magnetic properties of the CNT@MNP@mSiO<sub>2</sub> hybrid, showing magnetization as a function of magnetic field applied in range  $-20\text{ kOe}$  to  $20\text{ kOe}$ , as measured by SQUID magnetization measurement. CNT@MNP without silica layering is also presented for comparison. Inset shows the samples being attracted to a magnet for CNT@MNP@mSiO<sub>2</sub>. (b) Graph in the narrow magnetic field range, and (c) saturation magnetization,  $M_s$ , and coercive force,  $H_c$ , of the samples calculated from the graphs. (d)  $T_2$ -weighted images of CNT@MNP@mSiO<sub>2</sub> samples measured by a clinical 4.7T MR system, showing remarkable change in signal intensity depending on Fe concentration (numbered in each image), and (e) plotting of  $1/T_2$  with respect to Fe concentration, showing a linear relationship with  $R_2$  relaxivity of  $155.8\text{ Fe mM}^{-1}\text{ s}^{-1}$ . (f) In vivo  $T_2$ -weighted MRI images of liver (left) and kidney and spleen (right) before and after intravenous administration of CNT@MNP@mSiO<sub>2</sub> nanocarriers. 0.2 mL of sample solution prepared in a physiological saline at a concentration of  $500\text{ }\mu\text{g/mL}$  was administered to 25 g mouse.

used under general anesthesia using 1% isoflurane gas. Typically, the nanocarriers suspended in a physiological saline at  $500\text{ }\mu\text{g/mL}$  were administrated to ICR mice (25 g, 5 weeks of age) through tail vein injection at a volume of 0.2 mL per mice. The axial sections of the whole body of the mice were imaged.

## RESULTS AND DISCUSSION

First, the TEM image (Figure 1a) showed the typical morphology of CNTs used as the template of the hybrid nanocarriers, which revealed CNTs with lengths of submicrometers, the size range that has also been popularly researched for cellular transportation.<sup>17–19</sup> We further characterized the CNT@MNP@mSiO<sub>2</sub> hybrid nanocarriers. The TEM images of CNT@MNP (Figure 1b) clearly showed a number of spherical MNPs (size of 102 nm on average) decorating the outer surface of the CNT. TEM images of CNT@MNP@mSiO<sub>2</sub> (Figure 1c) showed the mesoporous

silica shell (indicated as arrows) enclosing the CNT@MNP with quite a uniform thickness. MNPs (darker dotted region, arrowheads) present inside were also revealed. For the purpose of comparison, CNT@mSiO<sub>2</sub> produced free of MNPs is also shown (Figure 1d). The hydrolysis of TEOS and subsequent condensation reaction should occur by a heterogeneous nucleation process. First, partially hydrolyzed TEOS molecules adsorb onto the CNT@MNP surface, after which a condensation reaction of neighboring silanol groups follows to form siloxane networks under basic conditions (pH 10–11).<sup>20</sup> The thickness of the mSiO<sub>2</sub> was measured to be  $18 \pm 5\text{ nm}$ . The hydrodynamic sizes of the nanocarriers were examined by DLS measurement (Figure 1e). The sizes were 726, 752, and 846 nm for CNT, CNT@MNP, and CNT@MNP@mSiO<sub>2</sub>, respectively, and the values are considered to reflect the length of nanotubes. This dimensional range (submicrometers,  $< 1\text{ }\mu\text{m}$ ) has also been reported elsewhere for CNTs and their hybrids developed for the use as drug delivery and imaging

systems, suggesting their usefulness in biomedical applications.<sup>21–23</sup> The phase of the products was analyzed by XRD (Figure 1f). XRD of pure CNT showed three peaks at  $2\theta = 25.99$ ,  $42.94$ , and  $53.63^\circ$ , characteristic of a graphite structure, and that of CNT@MNP gave additional peaks which were those of ferrite. The size of MNP calculated from the (311) peak in the XRD pattern using Scherrer's equation resulted in 10.6 nm, which corresponds well to the TEM image.<sup>24</sup> The XRD pattern of CNT@MNP@mSiO<sub>2</sub> showed a broad peak at  $2\theta \approx 22^\circ$ , confirming the amorphous state of SiO<sub>2</sub>.

FT-IR analysis of the nanomaterials was also carried out (see Figure S1a in the Supporting Information). IR spectrum of the CNT showed the bands at  $1633$  and  $1586\text{ cm}^{-1}$ , which were attributed to amide carbonyl and N–H in plane stretching, and that of CNT@MNP presented a strong band at  $600\text{--}560\text{ cm}^{-1}$ , characterizing Fe–O vibration related to the magnetic core particles.<sup>15</sup> The IR spectrum of CNT@MNP@mSiO<sub>2</sub> revealed bands associated with the Si structure (Si–O–Si asymmetric stretching at  $1073\text{ cm}^{-1}$ , Si–O–Si symmetric vibration at  $806\text{ cm}^{-1}$  and Si–OH stretching at  $953\text{ cm}^{-1}$ , and bending at  $463\text{ cm}^{-1}$ ). The mSiO<sub>2</sub>-covered CNT@MNP exhibited a highly negative zeta-potential ( $-43.6\text{ mV}$ ), which is ascribed to the presence of a bunch of hydroxyl groups (see Figure S1b in the Supporting Information). When the CNT@MNP@mSiO<sub>2</sub> hybrid was functionalized with amine group, the zeta-potential dramatically changed to a highly positive value,  $+33.7\text{ mV}$ . This switchable charge characteristic of the CNT@MNP@mSiO<sub>2</sub> hybrid nanocarrier, afforded by a simple surface treatment, should allow for the versatile loading of biomolecules in a broad range, from negative- to positive-charged biomolecules, thorough charge–charge interaction. The effects of mSiO<sub>2</sub> on mesoporosity were further characterized (Figure 1g). The nitrogen adsorption/desorption isotherm curve of the CNT@MNP@mSiO<sub>2</sub> hybrid represents a behavior typical of a mesoporous material, with a sharp upturn in the high relative pressure region, which was not readily observed in the CNT@MNP without mesoporous silica coating. The average pore size (PS), specific pore volume (SPV) and specific surface area (SSA) values are also presented (Figure 1h). The generated mesopores in the CNT@MNP@mSiO<sub>2</sub> hybrid nanocarrier showed an average size of  $3.67\text{ nm}$ . The SPV and SSA values for CNT@MNP@mSiO<sub>2</sub> were significantly enhanced, compared to those for CNT@MNP;  $0.024$  vs  $0.23\text{ cm}^3/\text{g}$  in SPV, and  $24.61$  vs  $66.68\text{ m}^2/\text{g}$  in SSA; whereas the surface area increase was only 3 times, the pore volume increase was as high as  $\sim 10$  times. The BET results indicate that the mesoporous silica coating endowed the magnetic CNTs with a high level of mesoporosity, which will provide great potential for loading small therapeutic molecules.

Along with the physicochemical properties, the magnetic properties of the CNT@MNP@mSiO<sub>2</sub> hybrid were characterized using SQUID magnetometry. Figure 2 shows the room-temperature magnetization hysteresis loops of the CNT@MNP and CNT@MNP@mSiO<sub>2</sub> with respect to the magnetic field applied ( $-20\text{ kOe}$  to  $20\text{ kOe}$  in Figure 2a and the narrower range  $-80$  to  $80\text{ Oe}$  in Figure 2b). On the basis of these hysteresis loops, the magnetization behavior of both nanomaterials demonstrated ferromagnetic properties (i.e., a narrow hysteresis loop and low coercivity),<sup>15,25</sup> identical to those of pure MNP. The saturation magnetization ( $M_s$ ) and coercive force ( $H_c$ ) were obtained from the curves (Figure 2c). The  $M_s$  of CNT@MNP is  $46.3\text{ emu/g}$ , smaller than that of bulk MNP ( $94\text{ emu/g}$ <sup>26</sup>), which can be attributed to the existence of CNTs,

i.e., the reduced mass fraction of magnetite crystallites and the possible strain between the magnetite nanoparticles and the CNT surface.<sup>27</sup> With the mesoporous silica coating, the  $M_s$  value decreased to  $27.1\text{ emu/g}$ , which is due to the shielding effect of silica layer of the MNPs as well as the reduction in mass fraction of MNPs. The  $H_c$  values of CNT@MNP and CNT@MNP@mSiO<sub>2</sub> were determined to be comparable. Although the magnetic properties of the CNT@MNP@mSiO<sub>2</sub> hybrid were reduced with respect to those of pure magnetite nanoparticles, the hysteresis behaviors were characteristic of ferromagnetic materials, and the  $M_s$  and hysteresis loop area still exhibited high levels.

We further determined whether CNT@MNP@mSiO<sub>2</sub> hybrid nanocarrier could be used as a contrast agent in magnetic resonance imaging (MRI). Different amount of the hybrid was dispersed in water solution (which thus containing varying Fe concentration, as determined by ICP-AES), and the image contrast was measured by a clinical 4.7T MR system at room temperature. As the superparamagnetic characteristics of the MNP nanocrystals accelerate the transverse relaxation of water protons, the CNT@MNP@mSiO<sub>2</sub> hybrid is considered to be used as a  $T_2$  contrast agent in MRI. The  $T_2$ -weighted images of the samples revealed remarkable change in signal intensity depending on the Fe concentration (Figure 2d). Meanwhile, the transverse relaxivity  $R_2$  ( $1/T_2$ ) measured on the samples was shown to have a linearity with increasing Fe concentration (Figure 2e), indicating that CNT@MNP@mSiO<sub>2</sub> hybrid generated MRI contrast on  $T_2$  weighted spin-echo sequence. The transverse relaxivity  $R_2$  of CNT@MNP@mSiO<sub>2</sub> hybrid was calculated to be  $155.8\text{ Fe mM}^{-1}\text{ s}^{-1}$ , which was comparable to the literature values,<sup>28–31</sup> particularly to those of CNT/MNP hybrids without the mesoporous silica layer. Wu et al. developed CNT/MNP system for  $T_2$ -contrast agents, and they reported the  $R_2$  relaxivity of  $175.5\text{ Fe mM}^{-1}\text{ s}^{-1}$ .<sup>29</sup> Lamanna et al. also produced CNT/MNP hybrids and showed the  $R_2$  value of  $103\text{ Fe mM}^{-1}\text{ s}^{-1}$ .<sup>30</sup> The relaxivity of CNT/MNP system also depends on size and relative mass of MNPs, with the highest  $R_2$  value of  $110\text{ Fe mM}^{-1}\text{ s}^{-1}$  reported by Jang et al.<sup>31</sup> Therefore, the in vitro results shown herein suggest that CNT@MNP@mSiO<sub>2</sub> hybrid nanocarrier can be used as a favorable  $T_2$  contrast agent. On the other hand, the longitudinal relaxivity  $R_1$  of the CNT@MNP@mSiO<sub>2</sub> hybrid nanocarrier was measured to be  $5.92\text{ Fe mM}^{-1}\text{ s}^{-1}$ , a value much lower than  $R_2$  value, as have also been reported elsewhere on the MNP/CNTs,<sup>30,32</sup> implying the currently developed nanocarrier would be more proper use as  $T_2$  contrast agent.

The results on magnetization hysteresis loop behavior and the MRI contrast image allow us to consider choosing the multifunctional nanocarriers for the applications of magnetism-related fields, such as hyperthermia thermoseed for cancer treatment, magnetic resonance diagnostics, stem cell separation and imaging, and remotely controlled magnetic drug delivery.<sup>33,34</sup> Among else, we investigated the possibility of the developed CNT@MNP@mSiO<sub>2</sub> nanocarriers for the in vivo MRI applications. The in vivo contrast-enhancing effect of the nanocarriers was evaluated in ICR mice with the 4.7 T MRI system. The  $T_2$ -weighted MRI images of mouse liver and kidneys and spleen before and after the administration of samples are presented (Figure 2f). After intravenous injection, the liver was darkened significantly in comparison with those without administration, but less obvious attenuation was observed for both kidney and spleen (indicated as arrows), showing a similar result to other reports where CNT/MNP was

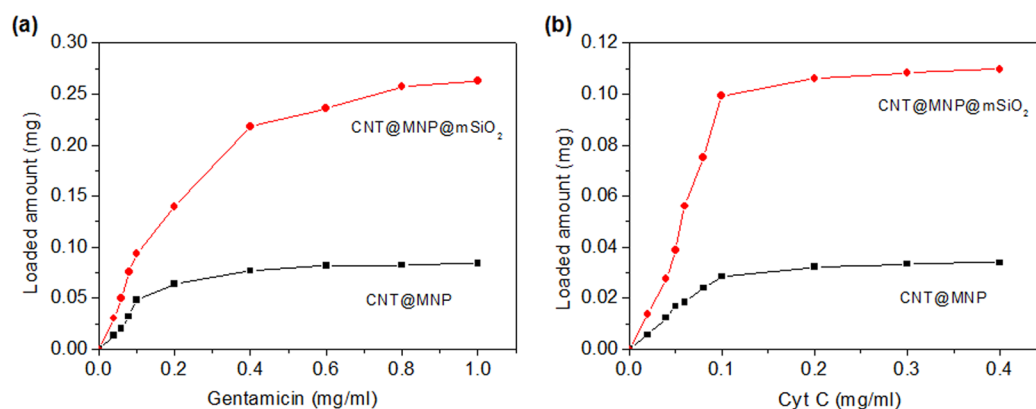


**Figure 3.** Loading capacity of therapeutic molecules onto the magnetic CNT due to the coverage of mesoporous silica; model biomolecules, including (a) gentamicin and (b) cyt C showed significant higher loading amount in CNT@MNP@mSiO<sub>2</sub> vs CNT-MNP.

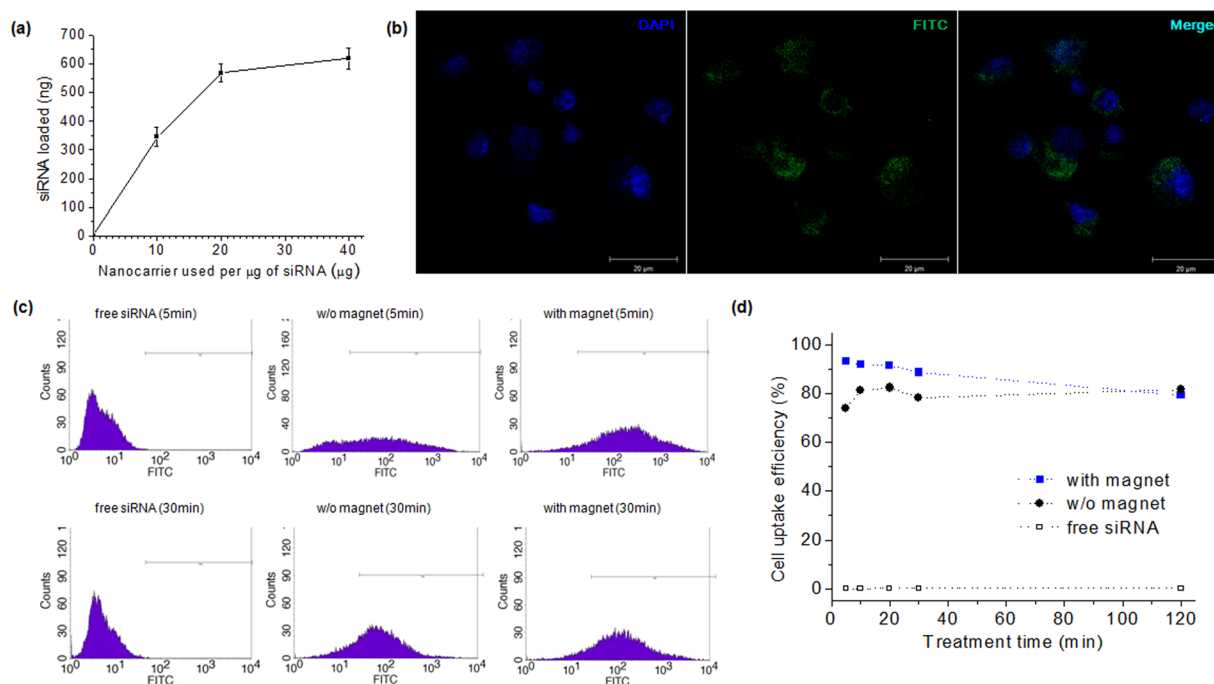


**Figure 4.** siRNA loading and cellular uptake study of the mesoporous magnetic CNT. (a) siRNA loaded amount with respect to varying quantity of the CNT@MNP@mSiO<sub>2</sub> nanocarriers (10, 20, and 40 μg used for each 1 μg of siRNA), showing an almost complete saturation at 20 μg. (b) Cell images taken by CLSM, fluorescence signals revealed for nuclei (blue, DAPI), siRNA-nanocarrier complex (green, FITC-conjugation to siRNA), and merged one. (c) Uptake efficiency measured by FACS analysis. Cellular uptake with or without magnet was carried out at varying time points, and cells positive for FITC signals were fluorescence-sorted. Free siRNA was used as a control. (d) Quantified graph of the uptake efficiency.

used.<sup>29</sup> The *in vivo* results suggest that the developed hybrid nanocarriers can act as a suitable negative ( $T_2$ ) contrast agent in MRI applications.

As another possible utility of the developed CNT@MNP@mSiO<sub>2</sub> hybrid nanocarrier, we here investigated the feasibility in loading therapeutic molecules and delivering them within cells through an intracellular penetration. Furthermore, for the loading study, we used three model biomolecules. As a model protein, cyt C was chosen, which is positive-charged and relatively small, compared to other proteins (molecular dimensions, 2.6 nm × 3.2 nm × 3.0 nm; and molecular weight, 886.90).<sup>35</sup> As a model small drug, gentamicin (the sulfated form) was selected, which is a hydrophilic antibiotic (molecular dimensions: 0.52 × 1.53 nm and molecular weight: 575.69).<sup>36</sup> Moreover, siRNA was chosen as a model nucleic acid, which is highly negatively charged and a relatively small nucleic acid

(~20 base pair). For the loading experiments, the charge–charge interactions between candidate molecules and mesoporous silica were considered, and thus, the as-layered *mSiO*<sub>2</sub> was used for both gentamicin and cyt C, whereas aminated-*mSiO*<sub>2</sub> was introduced for siRNA.

The capacity of the developed CNT@MNP@mSiO<sub>2</sub> hybrid for loading the model molecules was investigated. Figure 3 shows the loaded amount of gentamicin or cyt C within the CNT@MNP@mSiO<sub>2</sub>, as a function of the initial amount of model molecules used, and magnetic CNTs without *mSiO*<sub>2</sub> were compared. For both types of molecules, the saturated loading amount was significantly higher in CNT@MNP@mSiO<sub>2</sub> than in CNT-MNP; for gentamicin 0.27 vs 0.07 mg and for cyt C 0.11 vs 0.03 mg, showing approximately 4-fold increase in the loading capacity. Results clearly demonstrated the effective role of the mesoporous silica present on the

surface, in taking up model molecules within the mesopore structure. Gentamicin loading was much higher than cyt C loading, particularly on the CNT@MNP@mSiO<sub>2</sub> nanocarriers, which reflects the size effect of the molecules, i.e., smaller-sized gentamicin molecules are loaded to a greater degree within the mesopores of the silica.

For the loading of siRNA, we aminated the CNT@MNP@mSiO<sub>2</sub> samples to allow charge–charge interaction. In fact, the loading of siRNA onto the nonaminated CNT@MNP@mSiO<sub>2</sub> was found to be negligible. However, the aminated CNT@MNP@mSiO<sub>2</sub> clearly showed the incorporation of siRNA molecules (as shown in Figure 4a), signifying the importance of surface charges to effectively load nucleic acids. The amount of siRNA loaded was measured by a nanodrop method, by varying the quantity of CNT@MNP@mSiO<sub>2</sub> added initially (10, 20, and 40 μg) within the medium containing 1 μg of siRNA. Results indicated that almost complete saturation occurred through loading onto 20 μg of nanocarriers with approximately 0.6 μg saturated siRNA.

After confirming the siRNA loading onto the developed nanocarriers, we next sought to determine whether the siRNA-nanocarrier complex can be effectively delivered into tissue cells. Prior to this, we performed a cytotoxicity test to screen the doses of nanocarriers that are toxic to the cells. MC3T3-E1 cells were treated with the nanocarriers at varying doses (1 μg to 100 μg/mL) and the cell viability was measured at 24 h. Results gave dose-dependent cytotoxicity at doses largely above 10 μg/mL, below which the cells were almost intact (viability over 95% of blank control) (see Figure S2 in the Supporting Information). On the basis of this, we applied the dose of 10 μg/mL nanocarriers for the cellular uptake study. In particular, we designed a cell uptake study using a magnet, as the nanocarriers feature ferromagnetic properties. The cellular uptake of the siRNA-nanocarrier complex was visualized under a confocal microscope after FITC was conjugated to siRNA. Whereas the cells without siRNA loading did not show any fluorescence signals, those loaded with siRNA revealed strong green FITC-signals within the cytoplasm (Figure 4b). The cell-uptake efficiency of the siRNA-nanocarrier complex was analyzed by FACS (Figure 4c). Cells were treated either with siRNA only, or with the siRNA-nanocarrier complex, with or without the use of magnetism for different durations (5, 10, 20, 30, and 120 min). FACS histograms showed that large cell populations became positive for FITC-signals when treated with the siRNA-nanocarrier complex, which was not readily observed in the case of being treated with siRNA only. The cell-uptake efficiency of the delivery system was as high as ~72% at 5 min and ~80% at 120 min, even without the use of magnetism, which was further increased to 90–93% through the period when magnetism was introduced (Figure 4d). Results demonstrated the effectiveness of the developed CNT@MNP@mSiO<sub>2</sub> nanocarrier system in penetrating the cell membrane. Although the enhancement in the cellular uptake by the magnetism was not so big, the effect was also noticed, suggesting the role of MNPs embedded in the hybrid nanocarrier.

In fact, the cellular uptake of CNTs with nanotubular morphology has been confirmed in a range of studies.<sup>37–40</sup> Because of their needlelike shapes, CNTs are able to perforate cellular membrane and pass into the intracellular components very easily without causing apparent cell damage.<sup>37–40</sup> This is one merit of the currently developed CNT@MNP@mSiO<sub>2</sub> nanocarrier system with a nanotubular geometry that was

enabled by CNTs. In fact, because of the unique properties of CNTs, their biomedical applications have gained great attention, and particularly when developed to have multifunctionality, such as magnetism for diagnostics and mesoporosity for drug delivery, their potential for use in theranostics should be greatly improved. Here we demonstrated these aspects of CNTs with hybridization of MNPs and mSiO<sub>2</sub>. Future studies remain as to the specific applications of the developed nanocarriers, such as tissue repair and disease treatment, where the drug delivery and imaging capacities are on highly demand.

## CONCLUSIONS

In summary, we present a straightforward synthesis method of mesoporous magnetic CNT, CNT@MNP@mSiO<sub>2</sub>. The nanomaterial showed a high mesoporosity due to the surface-layered mSiO<sub>2</sub>, and excellent magnetic properties, retaining the characteristics of magnetite nanoparticles within the structure as revealed in vitro and in vivo. Investigation of the loading capacity of therapeutic molecules and their intracellular delivery demonstrated the mesoporous and magnetic nanocarriers showed high loading capacity for biological molecules, including gentamicin, cyt C, and siRNA, and allowed for a high cellular uptake rate through magnetism, while eliciting minimal toxicity to cells. This novel multifunctional nanocarrier may be potentially applicable as theranostic systems.

## ASSOCIATED CONTENT

### Supporting Information

FT-IR spectra and ζ-potential of samples (S1), and the cell viability of nanocarriers (S2). This material is available free of charge via the Internet at <http://pubs.acs.org/>.

## AUTHOR INFORMATION

### Corresponding Author

\*Tel: +82 41 550 3081. Fax: +82 41 550 3085. E-mail: kimhw@dku.edu.

### Notes

The authors declare no competing financial interest.

## ACKNOWLEDGMENTS

This work was supported by the Priority Research Centers Program (2009-0093829) through the National Research Foundation of Korea, Republic of Korea.

## REFERENCES

- (1) Iijima, S. Helical Microtubules of Graphitic Carbon. *Nature* **1991**, *354*, 56–58.
- (2) Tasis, D.; Tagmatarchis, N.; Bianco, A.; Prato, M. Chemistry of Carbon Nanotubes. *Chem. Rev.* **2006**, *106*, 1105–1136.
- (3) Hartmann, M. Ordered Mesoporous Materials for Bioadsorption and Biocatalysis. *Chem. Mater.* **2005**, *17*, 4577–4593.
- (4) Sing, R. K.; Kim, H. W. Inorganic Nanobiomaterial Drug Carriers Medicine. *Tissue Eng. Reg. Med.* **2013**, *10*, 296–309.
- (5) Zhang, L.; Qiao, S. Z.; Jin, Y. G.; Yang, H. G.; Budihartono, S.; Stahr, F.; Yan, Z. F.; Wang, X. L.; Hao, P. Z.; Lu, G. Q. Fabrication and Size-Selective Bioseparation of Magnetic Silica Nanospheres with Highly Ordered Periodic Mesostructure. *Adv. Funct. Mater.* **2008**, *18*, 3203–3212.
- (6) Morales-Cid, G.; Fekete, A.; Simonet, B. M.; Lehmann, R.; Carhenas, S.; Zhang, X.; Valcarcel, M.; Kopplin, P. S. In Situ Synthesis of Magnetic Multiwalled Carbon Nanotube Composites for the Cleanup of (Fluoro)Quinolones from Human Plasma Prior to Ultrahigh

Pressure Liquid Chromatography Analysis. *Anal. Chem.* **2010**, *82*, 2743–2752.

(7) Lee, P. L.; Chiu, Y. K.; Sun, Y. C.; Ling, Y. C. Synthesis of a Hybrid Material Consisting of Magnetic Iron-Oxide Nanoparticles and Carbon Nanotubes As a Gas Adsorbent. *Carbon* **2010**, *48*, 1397–1404.

(8) Wan, J. Q.; Cai, W.; Feng, J. T.; Meng, X. X.; Liu, E. Z. In Situ Decoration of Carbon Nanotubes with Nearly Monodisperse Magnetite Nanoparticles in Liquid Polyols. *J. Mater. Chem.* **2007**, *17*, 1188–1192.

(9) Liu, Y.; Jiang, W.; Xu, L.; Yang, X. W.; Li, F. S. Decoration of Carbon Nanotubes with Nearly Monodisperse  $M^{\text{II}}\text{Fe}_2\text{O}_4$  ( $M\text{Fe}_2\text{O}_4$ ,  $M = \text{Fe, Co, Ni}$ ) Nanoparticles. *Mater. Lett.* **2009**, *63*, 2526–2528.

(10) Liu, Z.; Yang, K.; Lee, S. T. Single-Walled Carbon Nanotubes in Biomedical Imaging. *J. Mater. Chem.* **2011**, *21*, 586–598.

(11) Yang, F.; Jin, C.; Yang, D.; iang, Y. J. J.; Li, J.; Di, Y.; Hu, J.; Wang, C.; Ni, Q.; Fu, D. Magnetic Functionalised Carbon Nanotubes As Drug Vehicles for Cancer Lymph Node Metastasis Treatment. *Eur. J. Cancer* **2011**, *47*, 1873–1882.

(12) Yang, D.; Yang, F.; Hu, J.; Long, J.; Wang, C.; Fu, D.; Ni, Q. Hydrophilic Multi-walled Carbon Nanotubes Decorated with Magnetite Nanoparticles As Lymphatic Targeted Drug Delivery Vehicles. *Chem. Commun.* **2009**, *29*, 4447–4449.

(13) Bottrill, M.; Green, M. Some Aspects of Quantum Dot Toxicity. *Chem. Commun.* **2011**, *47*, 7039–7050.

(14) Kwon, S.; Singh, R. K.; Perez, R. A.; Abou Neel, E. A.; Kim, H. W.; Chrzanowski, W. Silica-Based Mesoporous Nanoparticles for Controlled Drug Delivery. *J. Tissue Eng.* **2013**, *4*, 2041731413504777.

(15) Singh, R. K.; Kim, T. H.; Patel, K. D.; Knowles, J. C.; Kim, H. W. Biocompatible Magnetite Nanoparticles with Varying Silica Coating Layer for Use in Biomedicine; Physicochemical and Magnetic Properties and Cellular Compatibility. *J. Biomed. Mater. Res. A* **2012**, *100A*, 1734–1742.

(16) Deng, Y.; Deng, C.; Yang, D.; Wang, D.; Fu, S.; Zhang, X. Preparation, Characterization, and Application of Magnetic Silica Nanoparticle Functionalized Multi-Walled Carbon Nanotubes. *Chem. Commun.* **2005**, *44*, 5548–5550.

(17) Raffa, V.; Ciafani, G.; Nitodas, S.; Karachalios, T.; D'Alessandro, D.; Masini, M.; Cuschieri, A. Can the Properties of Carbon Nanotubes Influence Their Internalization by Living Cells? *Carbon* **2008**, *24*, 1600.

(18) Al-Jamal, K. T.; Nerl, H.; Muller, K. H.; Ali-Boucetta, H.; Li, S.; Haynes, P. D.; Jinschek, J. R.; Prato, M.; Bianco, A.; Kostarelos, K.; Porter, A. E. Cellular Uptake Mechanisms of Functionalised Multi-walled Carbon Nanotubes by 3D Electron Tomography Imaging. *Nanoscale* **2011**, *3*, 2627–2635.

(19) Lacerda, L.; Russier, J.; Pastorin, G.; Herrero, M. A.; Venturelli, E.; Dumortier, H.; Al-Jamal, K. T.; Prato, M.; Kostarelos, K.; Bianco, A. Translocation Mechanisms of Chemically Functionalised Carbon Nanotubes Across Plasma Membranes. *Biomaterials* **2012**, *33*, 3334–3343.

(20) Zou, H.; Wu, S.; Ran, Q.; Shen, J. A Simple and Low-Cost Method for the Preparation of Monodisperse Hollow Silica Spheres. *J. Phys. Chem. C* **2008**, *112*, 11623–11629.

(21) Skandani, A. A.; Zeineldin, R.; Al-Haik, M. Effect of Chirality and Length on the Penetrability of Single-Walled Carbon Nanotubes into Lipid Bilayer Cell Membranes. *Langmuir* **2012**, *28*, 7872–7879.

(22) Kam, N. W. S.; Dai, H. Carbon Nanotubes As Intracellular Protein Transporters: Generality and Biological Functionality. *J. Am. Chem. Soc.* **2005**, *127*, 6021–6026.

(23) Singh, R.; Pantarotto, D.; McCarthy, D.; Chaloin, O.; Hoebeke, J.; Partidos, C. D.; Briand, J.-P.; Prato, M.; Bianco, A.; Kostarelos, K. Binding and Condensation of Plasmid DNA onto Functionalized Carbon Nanotubes: Toward the Construction of Nanotube-Based Gene Delivery Vectors. *J. Am. Chem. Soc.* **2005**, *127*, 4388–4396.

(24) Hammond, C. *The Basics of Crystallography and Diffraction*; Oxford University Press: Oxford, U.K., 1997.

(25) Singh, R. K.; El-Fiqi, A. M.; Patel, K. D.; Kim, H. W. A novel preparation of magnetic hydroxyapatite nanotubes. *Mater. Lett.* **2012**, *75*, 130–133.

(26) Cullity, R. D. *Introduction to Magnetic Materials*; Addison-Wesley: Reading, MA, 1972.

(27) Rajendran, M.; Pullar, R. C.; Bhattacharya, A. K.; Das, D.; Chintalapudi, S. N.; Majumdar, C. K. Magnetic Properties of Nanocrystalline  $\text{CoFe}_2\text{O}_4$  Powders Prepared at Room Temperature: Variation with Crystallite Size. *J. Magn. Magn. Mater.* **2001**, *232*, 71–83.

(28) Lee, J. H.; Huh, Y. M.; Jun, Y.; Seo, J.; Jang, J.; Song, H. T.; et al. Artificially Engineered Magnetic Nanoparticles for Ultra-Sensitive Molecular Imaging. *Nat. Med.* **2006**, *13*, 95–99.

(29) Wu, H.; Liu, G.; Zhuang, Y.; Wu, D.; Zhang, H.; Yang, H.; Hu, H.; Yang, S. The Behavior after Intravenous Injection in Mice of Multiwalled Carbon Nanotube/ $\text{Fe}_3\text{O}_4$  Hybrid MRI Contrast Agents. *Biomaterials* **2011**, *32*, 4867–4866.

(30) Lamanna, G.; Garofalo, A.; Popa, G.; Wilhelm, C.; Begin-Colin, S.; Felder-Flesch, D.; Bianco, A.; Menard-Moyon, C. Endowing Carbon Nanotubes with Superparamagnetic Properties: Applications for Cell Labeling, MRI Cell Tracking and Magnetic Manipulations. *Nanoscale* **2013**, *5*, 4412–4421.

(31) Jang, J.; Nah, H.; Moon, S. H.; Kim, M. G.; Cheon, J. Critical Enhancements of MRI Contrast and Hyperthermic Effects by Dopant-Controlled Magnetic Nanoparticles. *Angew. Chem., Int. Ed.* **2009**, *121*, 1260–1264.

(32) Chen, Y.; Gu, H. Microwave Assisted Fast Fabrication of  $\text{Fe}_2\text{O}_3$ -MWCNTs Nanocomposites and Their Application as MRI Contrast Agents. *Mater. Lett.* **2012**, *67*, 49–51.

(33) Saavedra, F. M. M.; Hernandez, E. R.; Bore, A.; Arcos, D.; Vallet-Regi, M.; Vilaboa, N. Magnetic Mesoporous Silica Spheres for Hyperthermia Therapy. *Acta Biomater.* **2010**, *6*, 4522–4531.

(34) Sun, C.; Lee, J. S. H.; Zhang, M. Magnetic Nanoparticles in MR Imaging and Drug Delivery. *Adv. Drug Delivery Rev.* **2008**, *60*, 1252–1285.

(35) Vinu, A.; Murugesan, V.; Tangermann, O.; Hartmann, M. Adsorption of Cytochrome C on Mesoporous Molecular Sieves: Influence of PH, Pore Diameter and Aluminium Incorporation. *Chem. Mater.* **2004**, *16*, 3056–3065.

(36) Doadrio, A. L.; Sousa, E. M. B.; Doadrio, J. C.; Pérez Pariente, J.; Barba, I. I.; Vallet-Regi, M. Mesoporous SBA-15 HPLC Evaluation for Controlled Gentamicin Drug Delivery. *J. Controlled Release* **2004**, *97*, 125–132.

(37) Pantarotto, D.; Briand, J. P.; Prato, M.; Bianco, A. Translocation of Bioactive Peptides Across Cell Membranes by Carbon Nanotubes. *Chem. Commun.* **2004**, *10*, 16–17.

(38) Pantarotto, D.; Singh, R.; McCarthy, D.; Erhardt, M.; Briand, J.-P.; Prato, M.; Kostarelos, K.; Bianco, A. Functionalized Carbon Nanotubes for Plasmid DNA Gene Delivery. *Angew. Chem., Int. Ed.* **2004**, *43*, 5242–5246.

(39) Kam, N. W. S.; Liu, Z.; Dai, H. Carbon Nanotubes as Intracellular Transporters for Proteins and DNA: An Investigation of the Uptake Mechanism and Pathway. *Angew. Chem., Int. Ed.* **2006**, *45*, 577–581.

(40) Kam, N. W. S.; Liu, Z.; Dai, H. Functionalization of Carbon Nanotubes via Cleavable Disulfide Bonds for Efficient Intracellular Delivery of siRNA and Potent Gene Silencing. *J. Am. Chem. Soc.* **2005**, *127*, 12492–12493.